The effects of hydrogen addition on silica aggregate growth in atmospheric-pressure, 1-D methane/air flames with hexamethyldisiloxane admixture

Langenkamp, Peter N.; Levinsky, Howard B.; Mokhov, Anatoli V.

Published in:
International Journal of Hydrogen Energy

DOI:
10.1016/j.ijhydene.2017.12.022

Publication date:
2018

Available online at www.sciencedirect.com

ScienceDirect

journal homepage: www.elsevier.com/locate/he

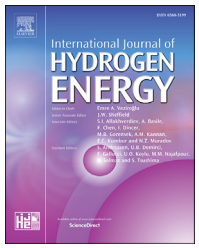

The effects of hydrogen addition on silica aggregate growth in atmospheric-pressure, 1-D methane/air flames with hexamethyldisiloxane admixture

Peter N. Langenkamp [a], *Howard B. Levinsky* [a,b], *Anatoli V. Mokhov* [a,*]

[a] *University of Groningen, Faculty of Science and Engineering, Energy and Sustainability Research Institute Groningen, Groningen, The Netherlands*

[b] *DNV GL, Oil & Gas, Groningen, The Netherlands*

ARTICLE INFO

Article history:
Received 28 September 2017
Received in revised form
29 November 2017
Accepted 4 December 2017
Available online 4 January 2018

Keywords:
Nanoparticles
Flames
Laser scattering
Fractal aggregates
Siloxanes

ABSTRACT

The effect of hydrogen addition on silica growth in burner-stabilized methane/air flames with trace amounts of hexamethyldisiloxane are reported. Profiles of the aggregates' radius of gyration R_g and monomer radius a versus residence time were measured by laser light scattering. Experiments were performed at equivalence ratios of 0.8, 1.0 and 1.3, with mole fractions of 0–0.4 of hydrogen in the fuel. At equal mass flux, the addition of hydrogen was found to result in decreasing R_g and a. However, keeping the flame temperature rather than the mass flux constant upon hydrogen addition resulted in the same measured profiles.

Introduction

Biogas is a compelling alternative to fossil fuels, and can play an important role in a transition to more sustainable energy production, but their utilization is often not straightforward. One major problem for utilizing biogas is that it contains high fractions of CO_2, which result in relatively low flame temperatures and burning rates, and a narrow range of flame stability [1]. To improve these unfavorable combustion characteristics of biogas, it is possible to blend it with another fuel. In particular, recent work with biogas has focused on improving the combustion characteristics by the addition of hydrogen [2–5], which if produced from renewable power maintains the sustainable character of the biogas. Facilitating these efforts, the combustion characteristics of hydrogen/hydrocarbon blends have been extensively studied (for example, with regards to burning velocity [6–10], ignition properties [11–13], flame stability enhancement [9,14–16], and the effect of hydrogen addition on NO and soot precursor formation [17–19]).

Another issue complicating the implementation of biogas in the energy infrastructure is the presence of trace compounds like siloxanes. Deleterious effects on the performance of combustion equipment caused by the deposition of the

* *Corresponding author.*
E-mail addresses: p.n.langenkamp@rug.nl (P.N. Langenkamp), Howard.Levinsky@dnvgl.com (H.B. Levinsky), a.v.mokhov@rug.nl (A.V. Mokhov).

https://doi.org/10.1016/j.ijhydene.2017.12.022
0360-3199/

silica particles generated by the combustion of siloxane-containing fuels put limits on acceptable concentrations of siloxane impurities [20]. It is important to note that these effects are not simply a function of the concentration of silica in the flue gases, but in fact, the structure of silica aggregates is a major determinant for the impact of deposition in combustion equipment. "Fluffy" fractal structures will block a larger volume, for example in a heat exchanger, than a denser layer of equal mass [21]. This underlines the importance of understanding what happens on the aggregate level.

Although many studies on silica aggregate growth have been performed both in hydrocarbon flames [22–27] and in hydrogen flames [28–32], to our knowledge there are no studies on the effect that hydrogen addition to hydrocarbon flames may have on the decomposition of the trace amount of silica-containing compounds in the fuel/oxidizer mixture and subsequent silica aggregate growth. Here, we investigate the effect of hydrogen addition on silica aggregate growth in burner-stabilized methane flames with hexamethyldisiloxane $C_6H_{18}Si_2O$ (abbreviated as L2) as silica precursor. Laser light scattering measurements are used to measure the development of the aggregates' radius of gyration R_g and the radius a of the primary particles (monomers) comprising these aggregates.

Setup and processing of scattering data

Silica aggregates were produced in atmospheric-pressure, flat premixed methane/hydrogen/L2/air flames, stabilized above a perforated ceramic burner deck. The burner system, gas supply and bubbler system used to add L2 to the gas mixture are identical to those used in our previous studies of silica aggregate growth in methane flames [27], with the exception of the addition of the supply of hydrogen and corresponding flow meter. The measurements of particle properties in the post-flame zone were performed by laser light scattering, using a setup similar to that used in our previous study [27]; in the current setup, we use a different laser (Viasho, 1 W at 532 nm). Axial profiles were obtained by moving the burner vertically relative to the laser beam. At each position, 60 measurements collected over the course of 1 min were averaged, resulting in a standard deviation of the measured scattering signal of typically less than 5%. The gyration radius R_g was determined using angle dependent light scattering, as described previously [27].

The primary particle radius a was determined from the scattering signal as follows. In general, the measured signal produced by scatterers with number density N, scattering the laser radiation of power P_L and wavelength λ at scattering angle θ, is given by:

$$I = c_0 P_L N \frac{d\sigma(\theta,\lambda)}{d\Omega} \quad (1)$$

where c_0 is a constant accounting for setup parameters, such as sampling volume, detector sensitivity and collection angle; and $\frac{d\sigma(\theta,\lambda)}{d\Omega}$ is the differential scattering cross section of the particles. For silica aggregates formed by monomers, assuming that there is no intracluster multiple scattering, the differential scattering cross section is given by Ref. [33]:

$$\frac{d\sigma_{SiO_2}(\theta,\lambda)}{d\Omega} = n^2 \frac{d\sigma^m_{SiO_2}}{d\Omega} S(q,R_g) \quad (2)$$

with $\sigma^m_{SiO_2}$ the scattering cross section of the individual monomers; n the number of monomers per aggregate; and $S(q,R_g)$ the structure factor, which is dependent upon the magnitude of the scattering wave-vector $q = \frac{4\pi}{\lambda}\sin\left(\frac{\theta}{2}\right)$. For small aggregates $S(q,R_g)$ can be approximated as $S \approx 1 + \frac{1}{3}q^2R_g^2/3$ [33] (this formula also forms the basis for the angle-dependent light scattering approach to measuring R_g used below [27]). The differential scattering cross section for a monomer with radius a and composed of a material with refractive index m, in turn, is [34]:

$$\frac{d\sigma^m_{SiO_2}}{d\Omega} = k^4 a^6 F(m) \quad (3)$$

where $k = \frac{2\pi}{\lambda}$, and $F(m) = \left|\frac{m^2-1}{m^2+2}\right|^2$. In the present work, we assume that the refractive index of the silica aggregates is approximately equal to that of silica glass at room temperature ($m \approx 1.5–10^{-7}$ i at 532 nm [35]). Taking into account the weak temperature dependence of the silica refraction index (~10^{-5} K^{-1} [36]) we expect only a small increase (no more than 5%) in $F(m)$ at flame temperatures in comparison to that at room temperature. Finally, combining Eqs. (1) through (3) gives the following expression for the measured signal produced by silica particles:

$$I_{SiO_2} = c_0 P_L k^4 F(m) S(q,R_g) N_{SiO_2} n^2 a^6 \quad (4)$$

where N_{SiO_2} is the number density of silica aggregates. In present work, c_0P_L is determined by measuring (at the same laser power P_L) the scattering signal I_{SF_6} from sulfur hexafluoride (SF_6) purged through the burner surface. From Eq. (1) it follows that

$$c_0 P_L = \frac{4\pi I_{SF_6}}{\sigma_{SF_6} N_{SF_6}} \quad (5)$$

where σ_{SF_6} is the total scattering cross section of SF_6 (3.23×10^{-26} cm^2 at 532 nm [37]), and N_{SF_6} the number density of SF_6 molecules.

Since the number of monomers inside an aggregate is related to a through $n = (R_g/a)^{D_f}$,where D_f is the fractal dimension [38] (which we assume to be approximately 1.8 [33]), we can write the following relation, expressing the monomer radius through experimentally determined parameters I_{SiO_2}, I_{SF_6} and R_g:

$$a = \left(\frac{\sigma_{SF_6} N_{SF_6} I_{SiO_2}}{3R_g^{D_f} I_{SF_6} k^4 F(m) S(q,R_g) f_v}\right)^{\frac{1}{3-D_f}} \quad (6)$$

where $f_v = \frac{4}{3}\pi n a^3 N_{SiO_2}$ is the silica volume fraction in the combustion products, which can be determined from the molar fraction of L2 in the fuel mixture if we assume that all silicon from L2 is fully oxidized to SiO_2, and subsequently fully condenses:

$$f_v = \frac{2\chi_{L2} M_{cp} M_{SiO_2} P}{M_{fuel/air} \rho_{SiO_2} RT} \quad (7)$$

Here χ_{L2} is the molar fraction of L2 in the fuel/air mixture; M_{cp}, M_{SiO_2} and $M_{fuel/air}$ the molecular masses of the combustion products, silica and the fuel/air mixture respectively; P the pressure; ρ_{SiO_2} the density of solid silica (where for the monomers we assume the silica bulk density of 2.65 g/cm^3 [39]); R the gas constant; and T the flame temperature. In the present work χ_{L2} and $M_{fuel/air}$ were calculated using the compositions of the unburned fuel/air mixture, while for calculations of M_{cp} the composition of the combustion products, obtained in numerical simulations (see below) was used.

Results and discussion

The measurements were performed for methane/hydrogen/L2/air mixtures in lean, stoichiometric and rich flames with varying fractions of H_2. The mass flux $\dot{M}$ was set to 0.0102 g/cm^{2}s for most flames. Provided that the fraction of L2 in the fuel β is small, the composition of the unburned fuel/air mixture can be chemically presented as

$$\phi\cdot(1-\gamma)CH_4+\phi\cdot\gamma\cdot H_2+\phi\cdot\beta\cdot L2+\left(2-\frac{3}{2}\gamma\right)O_2+3.77\cdot\left(2-\frac{3}{2}\gamma\right)N_2 \quad (8)$$

where ϕ is the fuel equivalence ratio, and γ the fraction of hydrogen in the fuel. An overview of the flame conditions examined here is given in Table 1. To facilitate the analysis of the experimental results, one-dimensional flame calculations were performed using the code from the Cantera suite [40] with the GRI-Mech 3.0 chemical mechanism [41]. Additional calculations were performed with the Konnov mechanism [42] showing only small temperature differences with GRI-Mech 3.0 of within 30 K. At mole fractions in this research of up to about 800 ppm in the unburned gas mixture, the concentration of L2 is too low to have a significant influence on the combustion properties [43]. It should be pointed out that extended experimental verifications [18,44] showed excellent agreement (within 30 K) between the measured and calculated temperature profiles in these flames. The computed flame temperatures at height of 1 cm above the burner deck and concentrations of SiO_2 molecules derived based on the calculated flame composition at the same height, are also presented in Table 1. The calculations indicate that the influence of hydrogen addition at fixed $\dot{M}$ and ϕ on flame temperature is modest for small values of γ. For example, for the highest value in this study of $\gamma = 0.4$, the flame temperature at 1 cm above the burner for $\phi = 1$ and $\dot{M} = 0.0102$ g/cm^{2}s drops from 1855 K to 1805 K (see Table 1). We note here that the apparently counterintuitive result of hydrogen addition resulting in a lower flame temperature arises from the use of burner-stabilized flames. At constant mass flux, the increase in free-flame burning velocity caused by hydrogen addition [18] requires heat transfer from the flame to the burner to reduce this higher burning velocity to the extant mass flux [45].

Axial profiles of R_g and a were obtained up to a maximum distance of 30 mm above the burner deck, as heat losses and mixing with surrounding air can only be neglected up to a limited height [46]. Stray light scattered from the burner setup limited the measurements to heights >8 mm above the burner surface. To facilitate the comparison of R_g and a obtained in flames with different gas velocities in the post-flame zone, the axial positions are recalculated to residence times using temperatures and compositions from 1-D simulations. Similar to what was reported in previous work [27], a small part of the data was acquired outside the regime of $qR_g \leq \sqrt{3}$ that is known to yield accurate R_g [33,47]. Because the plots of $I(0)/I(q)$ versus q^2 remain linear, it is expected that fits still give reliable values for R_g [33]. The full set of experimental data can be found in Appendix A.

Dependence of aggregate size on hydrogen fraction

The measured gyration radii R_g of silica aggregates produced by 6000 ppm L2 in the fuel in stoichiometric flames with $\dot{M} = 0.0102$ g/cm^{2}s are shown in Fig. 1, for $\gamma = 0$, 0.2 and 0.4 (flames A, B and D in Table 1). R_g is observed to grow with time for all hydrogen fractions. For example, at $\gamma = 0.4$ R_g increases from approximately 35 nm at a residence time t_{res} of 18 ms–105 nm at 55 ms. In addition, particles in flames with higher hydrogen fraction are consistently larger when compared at equal t_{res} (approximately by 10% and 20% for

Table 1 – Flame conditions used in this work.

Flame	ϕ	γ	β(ppm)	ξ(ppm)[a]	$\dot{M}/10^{-2}$g/cm^{2}s	T(K)
A	1	0	6000	1140	1.02	1855
B	1	0.2	6000	1330	1.02	1835
C	1	0.3	6000	1450	1.02	1820
D	1	0.4	6000	1600	1.02	1805
E	1	0	7020	1330	1.02	1855
F	1	0	7670	1450	1.02	1855
G	1	0	8460	1600	1.02	1855
H	1	0.2	6000	1330	1.08	1850
I	1	0.3	6000	1450	1.13	1850
J	1	0.4	6000	1600	1.23	1855
K	0.8	0.2	6000	1090	1.09	1715
L	0.8	0	7030	1090	1.02	1715
M	1.3	0.2	6000	1680	1.17	1875
N	1.3	0	7010	1680	1.02	1875

[a] ξ is the fraction of silica in the combustion products.

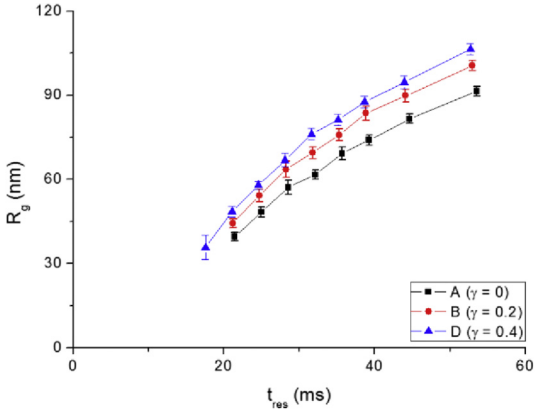

Fig. 1 – Radius of gyration R_g as function of residence time t_{res} for stoichiometric flames A, B and D with hydrogen fuel fractions $\gamma = 0$, 0.2 and 0.4.

$\gamma = 0.2$ and 0.4, respectively, compared to $\gamma = 0$ at all residence times). Neglecting for the moment the influence of γ on flame temperature, we might be able to attribute the change in R_g to the influence of the concentration ξ of silica in the combustion products. It is known that at constant temperature R_g increases with the concentration of precursor molecules when the growth of particles takes place through collisions [48]. Since the amount of air needed for a given equivalence ratio decreases with increasing hydrogen fraction (Eq. (8)), a constant siloxane fraction in the fuel will result in a higher SiO_2 fraction in the burned gases, as seen in Table 1. Thus, we expect higher γ to result in larger particles.

To test this expectation, we performed additional measurements of R_g in pure CH_4 flames with silica fractions in the combustion products matching those of the flames with added hydrogen. A comparison between flame D ($\gamma = 0.4$) and its corresponding reference flames A and G is presented in Fig. 2. Contrary to our expectations, the measurements (which are also representative for what is observed for lower hydrogen fractions) show a large difference in R_g between flames D and G with equal concentration of silica in the combustion products ($\xi = 1600$ ppm). Increasing ξ in the pure methane flame from 1140 to 1600 ppm resulted in gyration radii R_g larger than those in the hydrogen flame D, while for the same fraction in the fuel (β) lower R_g are observed. However, we cannot exclude the influence of temperature. Even though the change in flame temperatures upon hydrogen addition is ≤ 50 K, based on the earlier examination of its influence on silica aggregate growth [27], the observed differences in R_g might by fully attributable to this relatively modest change in flame temperature.

Additional measurements were performed at higher mass flux with added hydrogen (flames H, I and J in Table 1), with compositions matching flames B, C and D, and temperatures close to those of flames E, F and G without hydrogen. The results, presented in Fig. 3 as function of t_{res} (results for $\gamma = 0.3$ are omitted for clarity, but can be found in Appendix A), show excellent agreement with the radii measured in the flames with the same temperatures and total SiO_2 mole fraction in

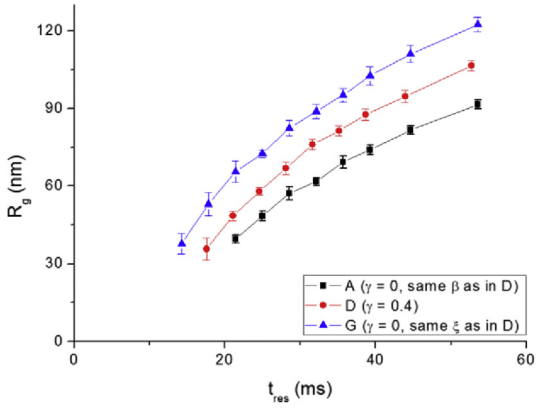

Fig. 2 – Radius of gyration R_g as function of residence time t_{res} for stoichiometric flames: flame D with hydrogen fuel fraction $\gamma = 0.4$ and two methane/air flames, one with the same concentration of L2 in fuel β (flame A) and the other with the same concentration of silica in the combustion products ξ (flame G).

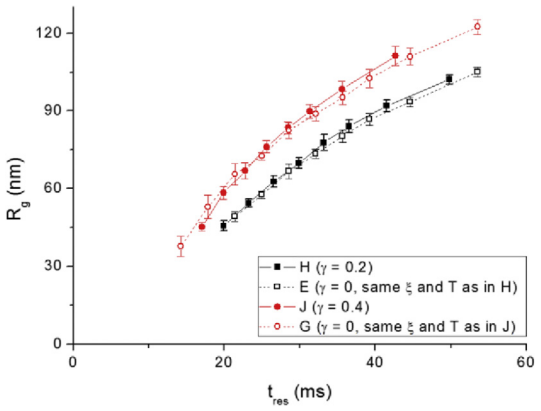

Fig. 3 – Radius of gyration R_g for stoichiometric flames H and J with hydrogen fuel fractions of 0.2 and 0.4, respectively, and corresponding reference flames E and G with equal concentration of silica in the combustion products ξ, all at $T = 1855$ K.

the combustion products. This demonstrates that the difference between particle size in flames with and without added hydrogen, at equal mass flux, arises entirely from the difference in flame temperature. The results indicate that the change in chemical environment due to the addition of hydrogen does not affect the process of silica aggregate growth.

Monomer size

The measured primary particle radii a in flames A, B and D are shown in Fig. 4 as a function of t_{res}. As follows from Equation (6), the standard deviation of a is determined by noise in I_{SiO_2}, I_{SF_6} and R_g. The standard deviations of the measured a (~10%) are also shown in the figure. The monomer radius is seen to follow the trend in R_g, being larger for higher hydrogen fractions, and growing with time. Although the observed growth is generally within the measurement uncertainty, the trend (~16% increase from 20 to 55 ms) was observed for all flames. Most interesting is that this growth occurs despite the relatively low flame temperatures (around 1855 K), which is well

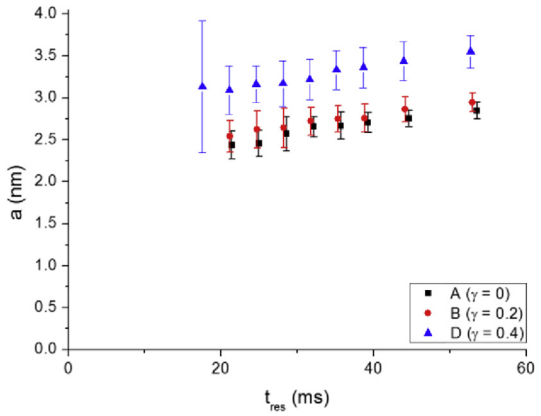

Fig. 4 – Monomer radius a as function of residence time t_{res} for stoichiometric flames A, B and D with hydrogen fuel fractions $\gamma = 0$, 0.2 and 0.4.

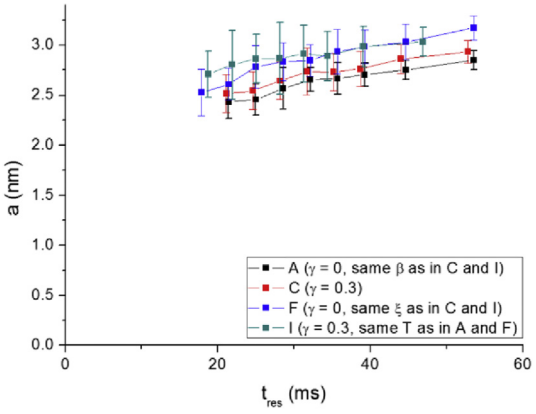

Fig. 5 – Monomer radius *a* as function of residence time t_{res} for stoichiometric flames: flames C and I with hydrogen fuel fraction $\gamma = 0.3$ and two methane/air flames, one with the same concentration of L2 in fuel β (flame A) and another with the same concentration of silica in the combustion products ξ (flame F).

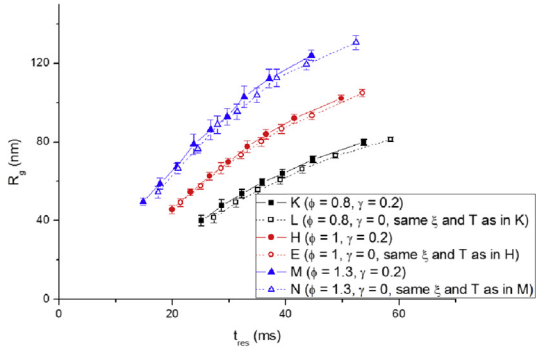

Fig. 6 – Radius of gyration R_g as function of residence time t_{res} for hydrogen/methane/air flames with $\gamma = 0.2$ and methane/air flames at $\phi = 0.8$ (flames K and L), $\phi = 1.0$ (flames E and H) and $\phi = 1.3$ (flames M and N). The methane/air flames have the same temperature and concentration ξ of silica in the combustion products as the corresponding flames with added hydrogen of the same ϕ.

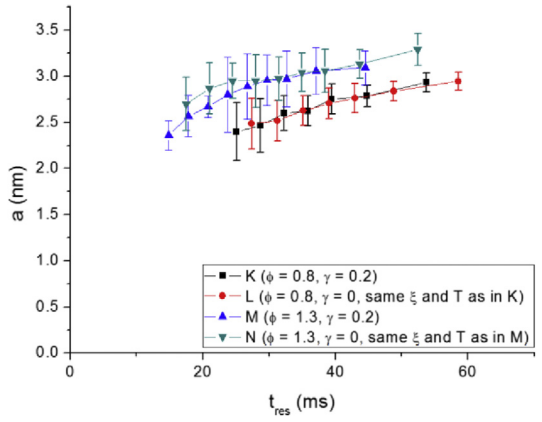

Fig. 7 – Comparison of monomer radius *a* as function of residence time t_{res} for lean flames at $\phi = 0.8$ with hydrogen fuel fraction $\gamma = 0.2$ (flame K) and pure methane/air flame with equal concentration of silica in the combustion products ξ and flame temperature (flame L), and rich flames at $\phi = 1.3$ with $\gamma = 0.2$ (flame M) and pure methane/air flame with equal ξ and flame temperature (flame N).

below the melting temperature of quartz [49] where the sintering process that is responsible for monomer growth would be expected to be very slow. Also, the effect of the change in flame temperature caused by hydrogen addition on monomer radius appears similar to what was observed for R_g; a typical example is shown in Fig. 5 for $\gamma = 0.3$.

We note that the initial monomer radii reported here are in good agreement with those observed in TEM measurements by Smirnov et al. [26] performed in a siloxane-doped methane/air flame, but that the growth observed here is much slower than that observed previously, where monomer radii larger than 7 nm were observed for similar t_{res}. Lack of reliable data regarding the properties of silica particles used in the analysis of the data presented above, such as density and refraction index, at the high temperatures encountered here complicates the discussion of the attendant uncertainties. However, we also note that the measurements by Smirnov et al. were performed in flames that were >200 K hotter and with a lower silicon fraction than those studied here. While the higher temperature could account for faster monomer growth, possible limitations of the sampling technique (which does not instantaneously freeze the particles, allowing for further growth during the sampling process) preclude further comparison. Further study is needed to provide a clear description of the impact of flame conditions on monomer growth.

Effect of equivalence ratio

The effect of hydrogen addition was also studied in lean ($\phi = 0.8$) and rich ($\phi = 1.3$) flames. Initially, the measurements were performed in flames of the same mass flux and concentration of L2 in the fuel mixture. This constant mass flux inevitably results in different temperatures ($T = 1715$ K, 1855 K and 1875 K for $\phi = 0.8$, 1 and 1.3, respectively, see Table 1). The axial profiles of R_g, presented in Fig. 6, show strong differences between particle sizes in flames of different equivalence ratios, reasonably consistent with the changes in R_g with flame temperature seen in the stoichiometric flames. Similar to the results obtained for the stoichiometric flames, the axial profiles in the lean and rich flames show very good agreement between the flames with and without added hydrogen at equal temperature and silica concentration in the combustion products. Thus, there is no indication of any impact of hydrogen addition on silica aggregate growth, except through changing the flame temperature.

The measured primary particles' radii *a* in lean and rich flames are shown in Fig. 7. The observed growth in primary particle radius with time for the various conditions is similar to that shown in Fig. 5 for the stoichiometric flames.

Conclusions

The effect of hydrogen addition on silica aggregate growth in CH_4/hexamethyldisiloxane/air burner-stabilized flames was

studied in flames of equivalence ratio $\phi = 0.8$, 1.0 and 1.3. At equal mass flux and silica concentration in the combustion products, hydrogen addition was found to result in decreasing aggregate sizes compared to the equivalent methane/air flames. The results show that this difference in R_g is caused by the decrease in flame temperature with hydrogen addition for all three equivalence ratios. Measured primary particle sizes show similar trends. While the primary particle size observed close to the burner are similar to those measured by TEM in siloxane-doped methane/air flames, the growth in the radius of these particles is much slower than observed previously. This difference is provisionally ascribed to differences in sintering rate caused by the difference of 200 K between the conditions of the different experiments. The results indicate that the impact of hydrogen addition on silica aggregate and primary particle growth is caused by the changes in temperature, rather than a change in the chemical environment.

Appendix A. Supplementary data

Supplementary data related to this article can be found at https://doi.org/10.1016/j.ijhydene.2017.12.022.

REFERENCES

[1] Lee CE, Hwang CH. An experimental study on the flame stability of LFG and LFG-mixed fuels. Fuel 2007;86:649–55. https://doi.org/10.1016/j.fuel.2006.08.033.

[2] Porpatham E, Ramesh A, Nagalingam B. Effect of hydrogen addition on the performance of a biogas fuelled spark ignition engine. Int J Hydrogen Energy 2007;32:2057–65. https://doi.org/10.1016/j.ijhydene.2006.09.001.

[3] Leung T, Wierzba I. The effect of hydrogen addition on biogas non-premixed jet flame stability in a co-flowing air stream. Int J Hydrogen Energy 2008;33:3856–62. https://doi.org/10.1016/j.ijhydene.2008.04.030.

[4] Zhen HS, Leung CW, Cheung CS. Effects of hydrogen addition on the characteristics of a biogas diffusion flame. Int J Hydrogen Energy 2013;38:6874–81. https://doi.org/10.1016/j.ijhydene.2013.02.046.

[5] Wei ZL, Leung CW, Cheung CS, Huang ZH. Effects of H2 and CO2 addition on the heat transfer characteristics of laminar premixed biogas–hydrogen Bunsen flame. Int J Heat Mass Transf 2016;98:359–66. https://doi.org/10.1016/j.ijheatmasstransfer.2016.02.064.

[6] Milton BE, Keck JC. Laminar burning velocities in stoichiometric hydrogen and hydrogen and hydrocarbon gas mixtures. Combust Flame 1984;58:13–22. https://doi.org/10.1016/0010-2180(84)90074-9.

[7] Yu G, Law CK, Wu CK. Laminar flame speeds of hydrocarbon + air mixtures with hydrogen addition. Combust Flame 1986;63:339–47. https://doi.org/10.1016/0010-2180(86)90003-9.

[8] Halter F, Chauveau C, Djebaïli-Chaumeix N, Gökalp I. Characterization of the effects of pressure and hydrogen concentration on laminar burning velocities of methane-hydrogen-air mixtures. Proc Combust Inst 2005;30:201–8. https://doi.org/10.1016/j.proci.2004.08.195.

[9] Zhang Y, Wu J, Ishizuka S. Hydrogen addition effect on laminar burning velocity, flame temperature and flame stability of a planar and a curved CH4-H2-air premixed flame. Int J Hydrogen Energy 2009;34:519–27. https://doi.org/10.1016/j.ijhydene.2008.10.065.

[10] Ennetta R, Alaya M, Said R. Numerical study of laminar flame velocity of hydrogen-enriched methane flames using several detailed reaction mechanisms. Arab J Sci Eng 2017;42:1707–13. https://doi.org/10.1007/s13369-016-2275-3.

[11] Fotache CG, Kreutz TG, Law CK. Ignition of hydrogen-enriched methane by heated air. Combust Flame 1997;110:429–40. https://doi.org/10.1016/S0010-2180(97)00084-9.

[12] Gersen S, Anikin NB, Mokhov AV, Levinsky HB. Ignition properties of methane/hydrogen mixtures in a rapid compression machine. Int J Hydrogen Energy 2008;33:1957–64. https://doi.org/10.1016/j.ijhydene.2008.01.017.

[13] Cheng RK, Oppenheim AK. Autoignition in methane hydrogen mixtures. Combust Flame 1984;58:125–39. https://doi.org/10.1016/0010-2180(84)90088-9.

[14] Schefer RW. Hydrogen enrichment for improved lean flame stability. Int J Hydrogen Energy 2003;28:1131–41. https://doi.org/10.1016/S0360-3199(02)00199-4.

[15] Arteaga Mendez LD, Tummers MJ, Van Veen EH, Roekaerts DJEM. Effect of hydrogen addition on the structure of natural-gas jet-in-hot-coflow flames. Proc Combust Inst 2015;35:3557–64. https://doi.org/10.1016/j.proci.2014.06.146.

[16] Guiberti TF, Durox D, Scouflaire P, Schuller T. Impact of heat loss and hydrogen enrichment on the shape of confined swirling flames. Proc Combust Inst 2015;35:1385–92. https://doi.org/10.1016/j.proci.2014.06.016.

[17] Hu E, Huang Z, Zheng J, Li Q, He J. Numerical study on laminar burning velocity and NO formation of premixed methane-hydrogen-air flames. Int J Hydrogen Energy 2009;34:6545–57. https://doi.org/10.1016/j.ijhydene.2009.05.080.

[18] Sepman AV, Mokhov AV, Levinsky HB. The effects of hydrogen addition on NO formation in atmospheric-pressure, fuel-rich-premixed, burner-stabilized methane, ethane and propane flames. Int J Hydrogen Energy 2011;36:4474–81. https://doi.org/10.1016/j.ijhydene.2010.12.117.

[19] Mze Ahmed A, Mancarella S, Desgroux P, Gasnot L, Pauwels JF, El Bakali A. Experimental and numerical study on rich methane/hydrogen/air laminar premixed flames at atmospheric pressure: effect of hydrogen addition to fuel on soot gaseous precursors. Int J Hydrogen Energy 2016;41:6929–42. https://doi.org/10.1016/j.ijhydene.2015.11.148.

[20] Turkin AA, Dutka M, Vainchtein D, Gersen S, van Essen VM, Visser P, et al. Deposition of SiO2 nanoparticles in heat exchanger during combustion of biogas. Appl Energy 2014;113:1141–8. https://doi.org/10.1016/j.apenergy.2013.08.068.

[21] Gersen S, Visser P, van Essen VM, Dutka M, Vainchtein D, de Hosson JTM, et al. Effects of silica deposition on the performance of domestic equipment. Proc Eur Combust Meet 2013;6. P1-51.

[22] Ulrich GD, Riehl JW. Aggregation and growth of submicron oxide particles in flames. J Colloid Interface Sci 1982;87:257–65. https://doi.org/10.1016/0021-9797(82)90387-3.

[23] Flower WL, Hurd AJ. In situ measurement of flame-formed silica particles using dynamic light scattering. Appl Opt 1987;26:2236–9. https://doi.org/10.1364/AO.26.002236.

[24] Hurd AJ, Flower WL. In situ growth and structure of fractal silica aggregates in a flame. J Colloid Interface Sci 1988;122:178–92. https://doi.org/10.1016/0021-9797(88)90301-3.

[25] Chang H, Chang H, Hong H, Won Y. Optical characterization of the nonspherical aerosol particles generated by combustion. Environ Educ Res 1998;3:79–86.

[26] Smirnov BM, Dutka M, van Essen VM, Gersen S, Visser P, Vainchtein D, et al. Growth of fractal structures in flames with silicon admixture. EPL (Europhys Lett) 2012;98:66005. https://doi.org/10.1209/0295-5075/98/66005.
[27] Langenkamp PN, Mokhov AV, Levinsky HB. Angle-dependent light scattering study of silica aggregate growth in 1-D methane/air flames with hexamethyldisiloxane admixture: effects of siloxane concentration, flame temperature, and equivalence ratio. Combust Sci Technol 2017;189:132–49. https://doi.org/10.1080/00102202.2016.1193500.
[28] Zachariah MR, Chin D, Semerjian HG, Katz JL. Dynamic light scattering and angular dissymmetry for the in situ measurement of silicon dioxide particle synthesis in flames. Appl Opt 1989;28:530. https://doi.org/10.1364/AO.28.000530.
[29] Choi M, Cho J, Lee J, Kim HW. Measurements of silica aggregate particle growth using light scattering and thermophoretic sampling in a coflow diffusion flame. J Nanoparticle Res 1999;1:169–83. https://doi.org/10.1023/A:1010092113802.
[30] Wooldridge MS, Danczyk SA, Wu J. Demonstration of gas-phase combustion synthesis of nanosized particles using a hybrid burner. Nanostruct Mater 1999;11:955–64. https://doi.org/10.1016/S0965-9773(99)00376-1.
[31] Lee BW, Jeong JI, Hwang JY, Choi M, Chung SH. Analysis of growth of non-spherical silica particles in a counterflow diffusion flame considering chemical reactions, coagulation and coalescence. J Aerosol Sci 2001;32:165–85. https://doi.org/10.1016/S0021-8502(00)00054-9.
[32] Suh JS, Kim CS, Kim TO, Choi M. Structural and chemical characterization of SiO2/TiO2 multicomponent particles during aerosol formation in a coflow diffusion flame. Adv Powder Technol 2006;17:495–508. https://doi.org/10.1163/156855206778440561.
[33] Sorensen CM. Light scattering by fractal aggregates: a review. Aerosol Sci Technol 2001;35:648–87. https://doi.org/10.1080/02786820117868.
[34] Bohren CF, Huffman DR. Absorption and scattering of light by small particles. Wiley-VCH; 1998.
[35] Kitamura R, Pilon L, Jonasz M. Optical constants of silica glass from extreme ultraviolet to far infrared at near room temperature. Appl Opt 2007;46:8118. https://doi.org/10.1364/AO.46.008118.
[36] Wray JH, Neu JT. Refractive index of several glasses as a function of wavelength and temperature. J Opt Soc Am 1969;59:774. https://doi.org/10.1364/JOSA.59.000774.
[37] Sneep M, Ubachs W. Direct measurement of the Rayleigh scattering cross section in various gases. J Quant Spectrosc Radiat Transf 2005;92:293–310. https://doi.org/10.1016/j.jqsrt.2004.07.025.
[38] Mandelbrot BB. The fractal geometry of nature. New York: W.H. Freeman and Co.; 1982.
[39] Greenwood NN, Earnshaw A. Chemistry of the elements. 2nd ed. Oxford: Butterworth-Heinemann; 1997.
[40] Goodwin DG, Moffat HK, Speth RL. Cantera: an object-oriented software toolkit for chemical kinetics, thermodynamics, and transport processes. 2015.
[41] Smith GP, Golden DM, Frenklach M, Moriarty NW, Eiteneer B, Goldenberg M, et al. GRI-MECH 3.0 n.d. http://www.me.berkeley.edu/gri_mech/ [Accessed June 24, 2015].
[42] Konnov AA. Remaining uncertainties in the kinetic mechanism of hydrogen combustion. Combust Flame 2008;152:507–28. https://doi.org/10.1016/j.combustflame.2007.10.024.
[43] Chagger HK, Hainsworth D, Patterson PM, Pourkashanian M, Williams A. The formation of SiO2 from hexamethyldisiloxane combustion in counterflow methane-air flames. Symp Combust 1996;26:1859–65. https://doi.org/10.1016/S0082-0784(96)80007-5.
[44] Sepman AV, Toro VV, Mokhov AV, Levinsky HB. Determination of temperature and concentrations of main components in flames by fitting measured Raman spectra. Appl Phys B 2013;112:35–47. https://doi.org/10.1007/s00340-013-5389-2.
[45] Law CK. Combustion physics. Cambridge: Cambridge University Press; 2006.
[46] Sepman AV, Mokhov AV, Levinsky HB. Extending the predictions of chemical mechanisms for hydrogen combustion: comparison of predicted and measured flame temperatures in burner-stabilized, 1-D flames. Int J Hydrogen Energy 2011;36:9298–303. https://doi.org/10.1016/j.ijhydene.2011.04.198.
[47] Sorensen CM, Lu N, Cai J. Fractal cluster size distribution measurement using static light scattering. J Colloid Interface Sci 1995;174:456–60. https://doi.org/10.1006/jcis.1995.1413.
[48] Friedlander SK. Smoke, dust and haze: fundamentals of aerosol dynamics. Second. New York: Oxford University Press; 2000.
[49] Lide DR, editor. Handbook of chemistry and physics. 84th ed. London: CRC Press; 2003.